The Secret 'After Life' of Foraminifera: Big Things Out of Small

Jim Buckman [1],* , **Carol Mahoney** [2], **Christian März** [2] **and Thomas Wagner** [3]

1   Institute of GeoEnergy Engineering, EGIS, Heriot-Watt University, Riccarton, Edinburgh EH14 4AS, UK
2   School of Earth and Environment, University of Leeds, Leeds LS2 9JT, UK;
     dr.carol.mahoney@gmail.com (C.M.); c.maerz@leeds.ac.uk (C.M.)
3   The Lyell Centre, Heriot-Watt University, Riccarton, Edinburgh EH14 4AS, UK; t.wagner@hw.ac.uk
*   Correspondence: j.buckman@hw.ac.uk

Abstract: Calcareous and siliceous microorganisms are common components of mudrocks, and can be important in terms of stratigraphy and environmental interpretation. In addition, such microorganisms can have a significant 'after life', through post-mortem alteration, and represent a potential source of additional information about the diagenetic and deformation history of the rock unit. Some examples of the latter are illustrated in this study from foraminifera within a Cretaceous black shale of Colombia. This includes foraminifera tests acting as understudied repositories of authigenic calcite cement, and of elements such as Ba, Zn, Fe and S through the formation of baryte, sphalerite and iron sulphides (pyrite, marcasite). Such repositories, within the body chambers of foraminiferal tests, can provide important windows into the diagenetic processes within mudstones. If calcite cement is not recognised or separated from biogenic calcite, the depositional calcite budget can be easily overestimated, skewing the application of mudrock classification schemes, and affecting environmental interpretation including that of productivity. The elements Ba, Zn and Fe (often in ratio with Al) are commonly utilised as geochemical proxies of environmental parameters (productivity, bottom water redox conditions, etc.). Therefore, the presence of significant amounts of baryte, sphalerite and pyrite-marcasite (within foraminifera) should be noted and their origins (source and timing) investigated based on their spatial relationships before making environmental deductions based on geochemical analysis alone. Additionally, commonly observed marginal shell damage of many of the observed foraminifera is reported. We interpret this damage, for the first time, as an indicator of lateral dissolution, brought about by horizontal foreshortening during orogenesis. This is also supported by the occurrence of microscale anastomosing horizontal to inclined baryte-filled fractures within the mudstone matrix.

Keywords: Cretaceous; diagenesis; foraminifera; carbonate; sulphides; sulphates; foreshortening

1. Introduction

Calcareous and siliceous nano- and microorganisms such as coccolithophores, foraminifera, and various forms of spicule are common within many marine mudstones, where they can form a significant component of the rock fabric (Figure 1). Such fossilised remains of marine microorganisms can be important in terms of stratigraphy, environmental interpretation (temperature, salinity, anoxia), evidence of transportation and sediment reworking (winnowing), substrate consistency, flow dynamics, rates of sedimentation and as indicators of increased periods of productivity and nutrient upwelling [1–9].
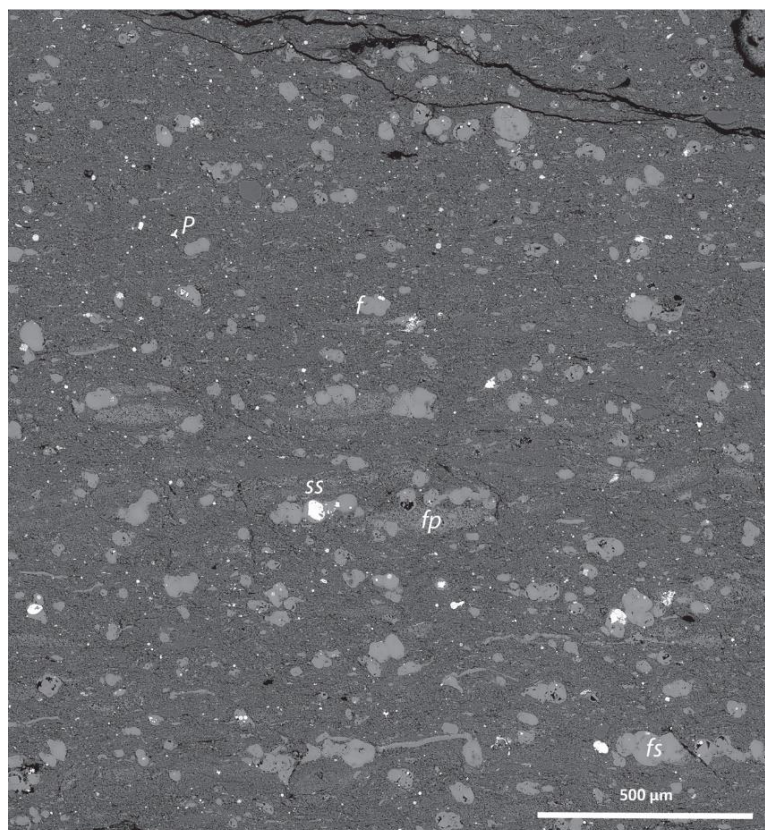
Figure 1. Backscattered electron (BSE) montage, illustrating the fabric of La Cristalina mudstone, with foraminifera (*f*), foraminifera stringers (*fs*), faecal pellets (*fp*), sulphides and sulphates (*ss*), and pyritised sponge spicule *(p)*.

The current paper illustrates an example of Cretaceous Colombian mudstone that contains foraminifera that display a range of interesting post-mortem features, (i) authigenic mineral infills within body chambers and (ii) unusual marginal damage of the tests. Previous studies within the Eagle Ford Formation (USA), from similar age and environment to the Colombian material, have indicated that calcite, kaolinite, pyrite and occasionally quartz can occur as infill within foraminifera chambers associated with organic material [10–12]. Herein, while kaolinite has not been observed, calcite, and pyrite are, with the addition of baryte, sphalerite and marcasite. Marginal damage of foraminifera tests appears not to have been previously reported elsewhere, including from the Eagle Ford Formation. Both the authigenic minerals and test damage are described herein, and discussed in terms of their potential significance. The purpose of the present paper is not to definitively answer all questions about sources, formation mechanisms and the ultimate meaning of these features, but instead to flag up areas of potential significance that may otherwise be overlooked. The aim is to stimulate further research and investigations.

2. Material and Methods

Here, we study a mudstone sample previously described from near La Cristalina (Figure 2), on the eastern side of the Middle Magdelena Valley (west of the Eastern Cordillera), Cretaceous of Colombia, South America [13]. It was imaged as a polished thin section by scanning electron microscopy (SEM), using a Quanta FEG 650 SEM (Thermo Fischer Scientific, Waltham, MA, USA), in the low-vacuum mode (0.82 Torr), operating at 20 kV, in association with energy dispersive X-ray (EDX) analysis, utilising an Oxford Instruments X-Max[N] 150 mm detector (Oxford Instruments NanoAnalysis & Asylum Research, High Wycombe, UK), with AZtec mapping and particle analysis software (Version 3.3, Oxford Instruments NanoAnalysis & Asylum Research, High Wycombe, UK). Backscattered electron

(BSE) imaging and EDX mapping were used in conjunction with gaseous secondary electron (GSE) imaging. The latter uses the charge contrast imaging (CCI) technique in order to elucidate details of shell morphology and the presence of calcite and quartz cements [13], which gives similar results to that of cathodoluminescence (CL) microscopy [14].
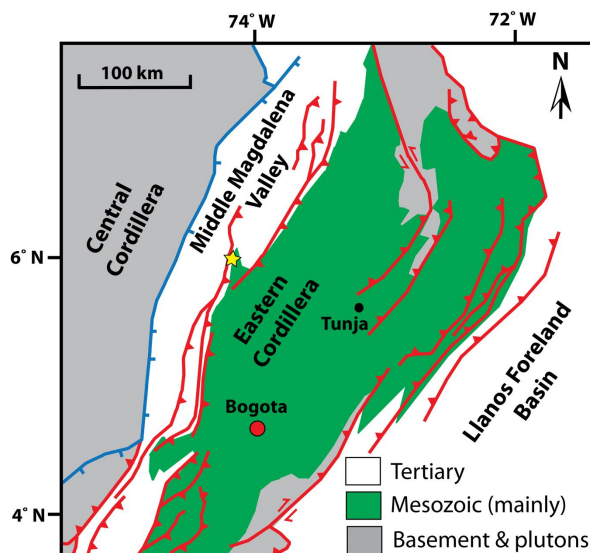

Figure 2. Locality map of the La Cristalina sample (yellow star), within its geographic, stratigraphic and structural context. Red lines = thrust faults; blue lines normal faults. After Giuliani et al. [15].

Polished thin sections were prepared using the following procedure. The sample was vacuum resin impregnated to fill any larger pores and stabilise the specimen. It was then trimmed to an appropriate size, using a diamond wafering saw and oil-based lubricating medium, to minimise damage to the mudstone microstructure. After fixation of the prepared sample to a glass thin section, the sample was machine polished to a thickness of 30 μm using a 600 grade aluminium oxide slurry. After cleaning, the sample was further hand polished using a series of diamond pastes, ending with a 1 μm paste. Hand polishing reduces plucking, and the diamond pastes produce a fine mirror-like surface suitable for elemental analysis and charge contrast imaging (CCI). Finally, the polished thin section was cleaned in an ultrasonic bath, using alcohol, to remove any remaining polishing agent. No coverslip was added, as the sample was destined for examination by scanning electron microscopy.

3. Results

Foraminifera are common features within the mudstone examined (Figure 1), occurring as isolated elements and as associated strings of crowded individuals, parallel to bedding. Many foraminifera are remarkably intact, show little evidence of flattening and have good preservation of shell microstructure. In some cases, the foraminifera chambers have acted as receptacles for authigenic calcite, FeS_2, iron oxide, sphalerite and baryte (Figure 3A–H). Calcite occurs as a coarse sparry infill (typically 10–20 μm), as a finer microspar (1 μm) coating the inner surfaces of foraminifera tests (Figure 3) and as a thin apparently structureless external layer around tests (Figure 4). Pyrite and iron oxides occur in the form of framboids (typically 5 μm diameter) and coarser equant crystals (up to ~10 μm). The latter often surround framboids and can totally infill foraminifera chambers. Sphalerite typically occurs as euhedral crystals (5 to 10 μm), surrounding pyrite framboids, and does not completely infill chambers (Figure 3). Baryte occurs as euhedral crystals (many up to 25 μm), and typically totally infills foraminifera chambers (Figure 3). Particle distribution analysis for FeS_2, iron oxides, sphalerite and baryte illustrates that all phases show some degree of overlap in terms of area of coverage (Figure 5). Baryte is the most pervasive and well distributed phase, while FeS_2, although more numerous, is restricted in terms of its distribution (Figure 5). Sphalerite has a similar distribution to that of FeS_2, but slightly more restricted, and iron

oxides occur as a halo around the area containing FeS_2. Some microquartz is also occasionally observed within foraminifera chambers (Figure 6). Although foraminifera in general are well preserved, many are notable for the occurrence of marginal damage to the test (Figures 4 and 6), which is always restricted to lateral areas within the plane of bedding. The use of charge contrast imaging (CCI) illustrates that both shell and calcite cements are missing from the margins of the tests (Figure 4F).
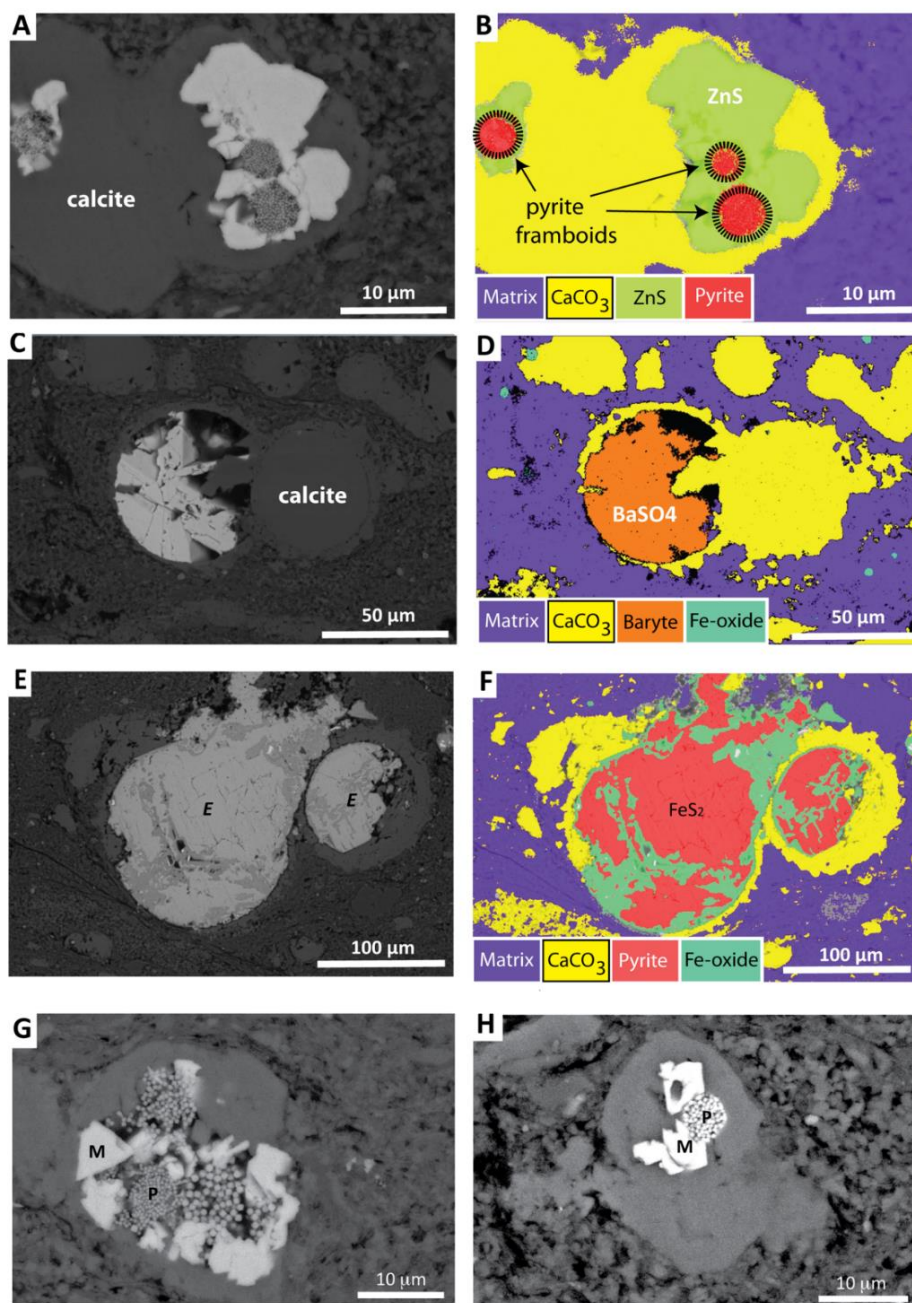
Figure 3. (**A,C,E,G,H**) Backscattered electron (BSE) images of typical foraminifera and associated secondary minerals. (**B,D,F**) Energy dispersive X-ray (EDX) phase maps of (**A,C,E**), showing calcite cement (**B,D**), pyrite framboids (**B**), highlighted by dashed black circles, euhedral sphalerite (**B**), baryte (**D**), and euhedral pyrite/Fe oxide (hydroxide) (**F**)—with iron oxide in dark green. Further, small oxidised pyrite framboids are shown in (**D**). (**G,H**) Foraminifera with calcite cement, and FeS_2 in the form of pyrite framboids (*P*) and larger euhedral "marcasite" (*M*). Note, that differentiation between calcite test and authigenic calcite is more clearly illustrated in the charge contrast images (CCIs) in Figures 4 and 6.
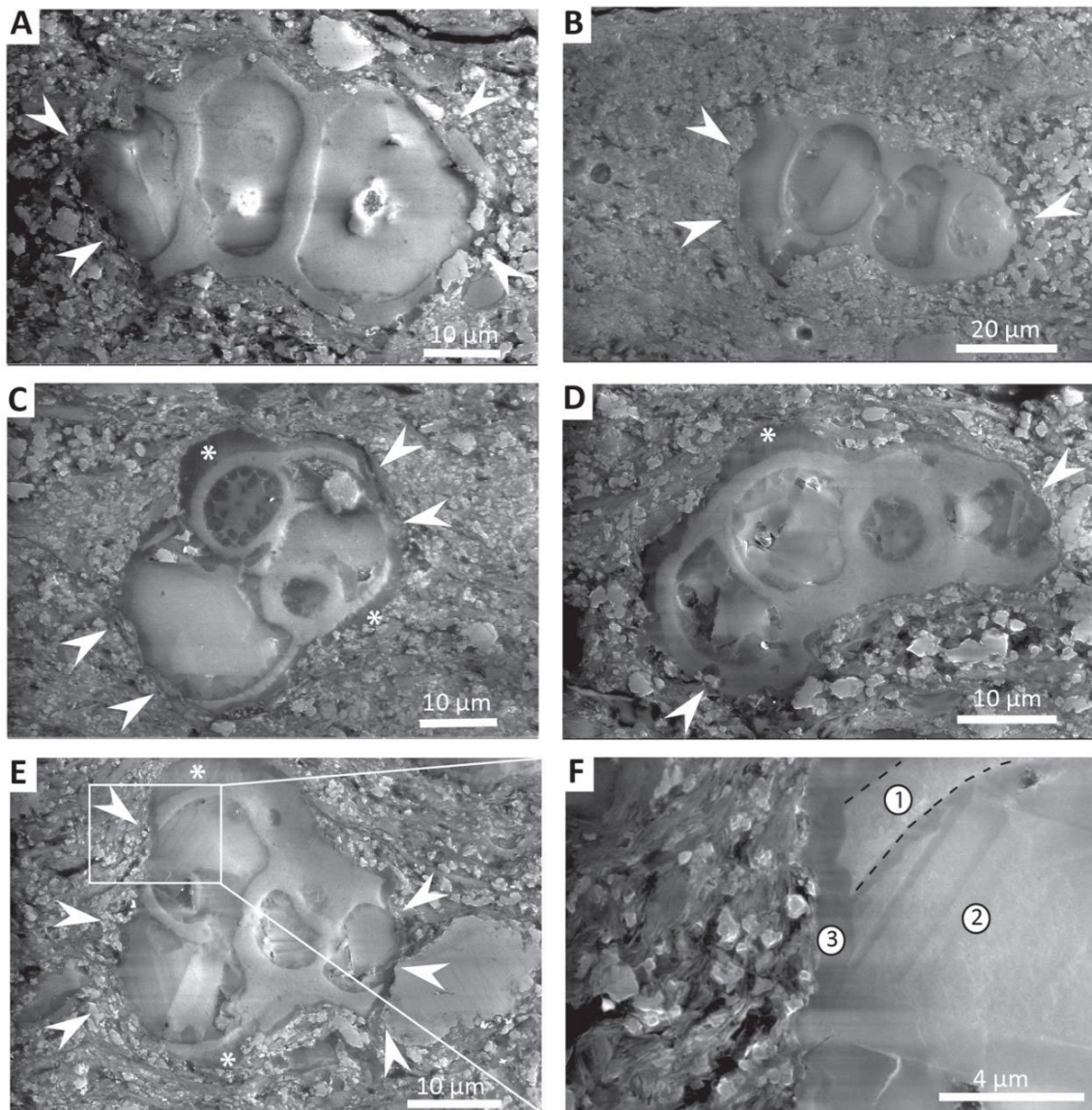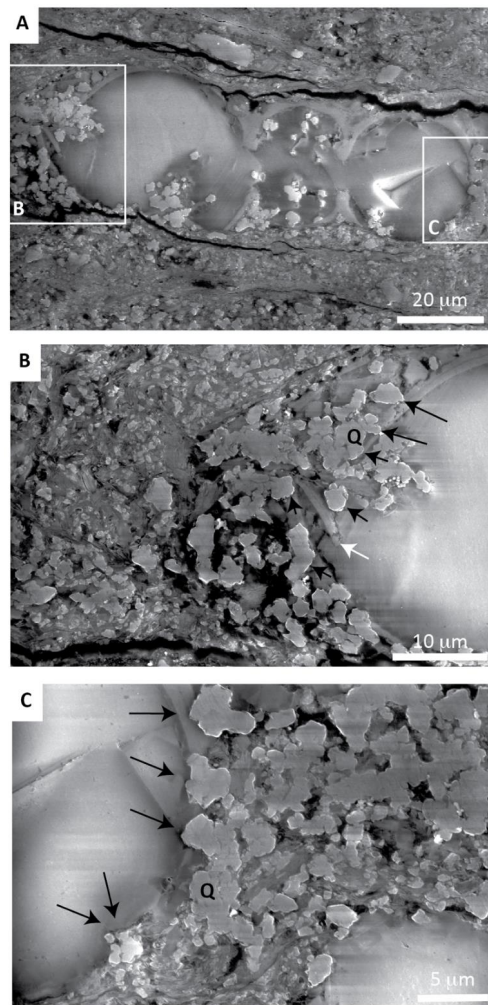
Figure 4. Gaseous secondary electron (GSE) charge contrast images (CCIs) showing the presence and nature of calcite cement, and lateral dissolution of foraminifera tests. Bedding is approximately horizontal in all images. (**A–E**) Individual examples displaying areas of peripheral damage due to horizontal foreshortening. All individuals are filled with calcite cement, with two phases of cement clearly observed in (**C,D**). Asterisk marks locations where calcite cement is thickly developed on the upper and lower surfaces of the test. (**F**) Enlargement of area marked in (**E**). 1—calcite test; 2—sparry calcite cement within test; 3—calcite cement on outer surface of test, and on broken test and inner sparry cement surfaces (post-dissolution). Note the scalloped dissolution surface between 3 and 1, as well as 3 and 2.
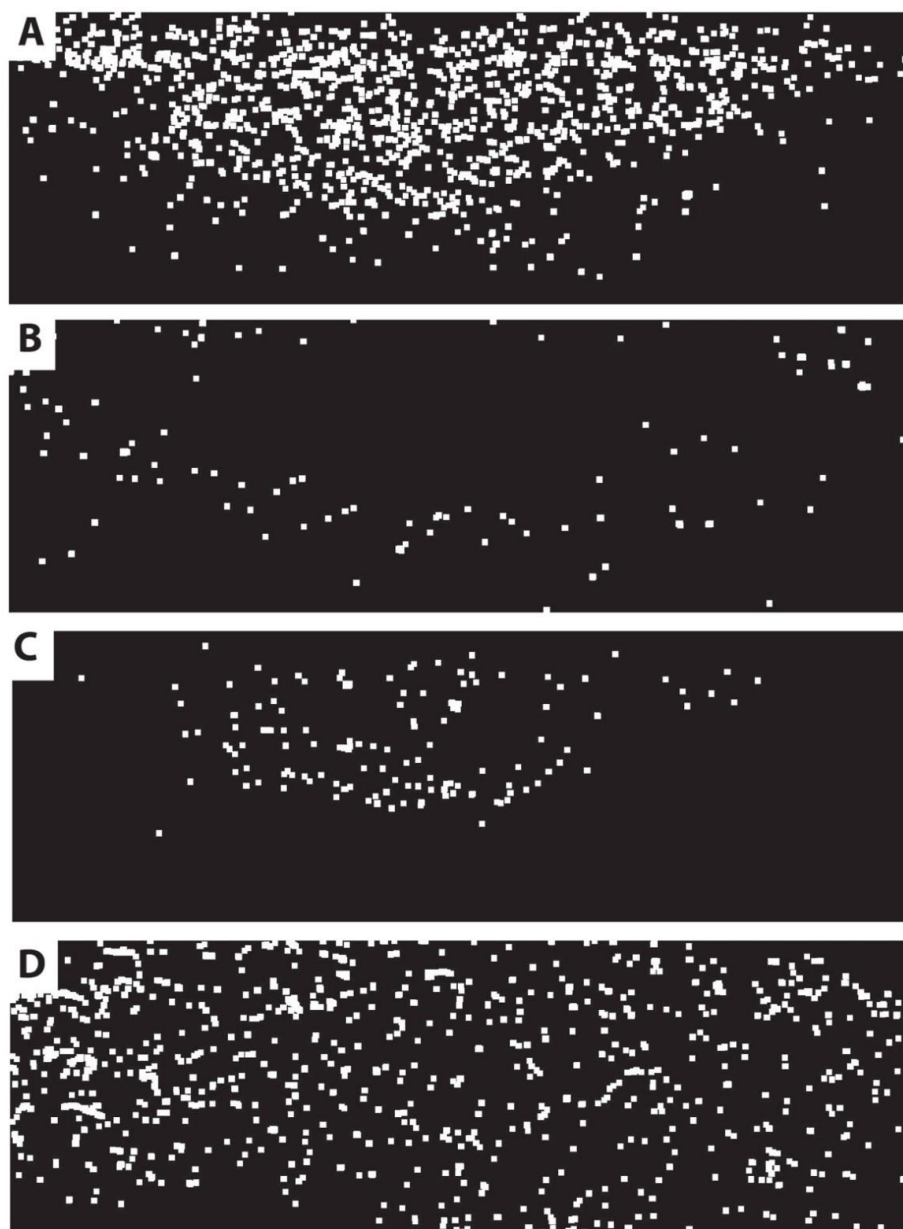
Figure 5. Phase distribution maps (across whole thin section), constructed using AZtec Feature and processed in ImageJ, for (**A**) pyrite (includes "marcasite"), (**B**) iron oxide, (**C**) sphalerite and (**D**) baryte. Horizontal field of view is approximately 40 mm. Note that dots only mark the relative position of phases, and are not to scale (pixels dilated four times to help with visualisation). Sulphides are both restricted, particularly sphalerite. Iron oxides form a halo around the area dominated by pyrite. Baryte has a more pervasive widespread distribution.

Within the mudstone matrix, FeS_2 framboids and isolated euhedral crystals are also present. However, the dominant authigenic phase is that of microquartz, which is pervasive and occurs as pore-filling cement and overgrowths to detrital silt grains [13]. Calcite cement is lacking, apart from where it occurs as syntaxial overgrowths of coccolithophore plates within faecal pellets (Figure 7). In addition, baryte is also seen to occur as the fill of horizontal to subhorizontal anastomosing microcracks (Figure 8).

Figure 6. Gaseous secondary electron (GSE), charge contrast images (CCIs) showing lateral dissolution of foraminifera tests. Bedding is approximately horizontal in all images. (**A**) Overview (note some basal dissolution due to burial loading); (**B**,**C**) details of areas marked in (**A**). Q = microquartz cement. Arrows indicate shell dissolution where microquartz contacts foraminifera test. Note some limited mechanical breakage (white arrow).
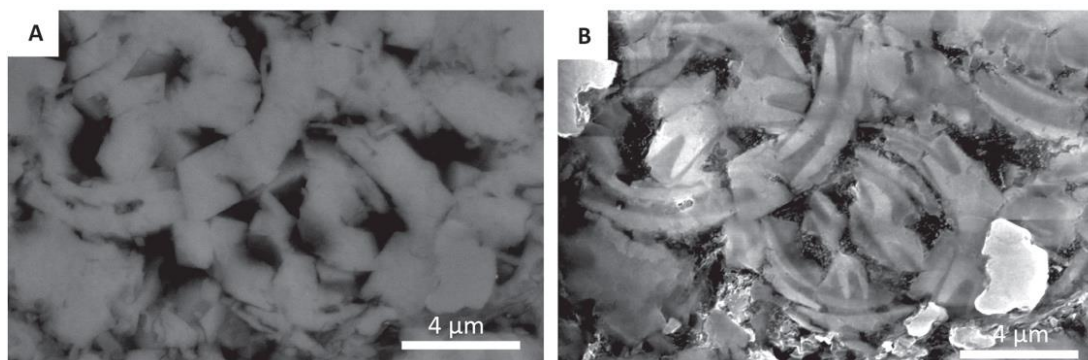
Figure 7. (**A**) Backscattered electron (BSE) and (**B**) gaseous secondary electron (GSE) charge contrast image (CCI) pair of details within faecal pellets, showing disarticulated coccolithophore plates. Note the blocky nature of calcite in (**A**), representing coccolithophore plates plus syntaxial cement, and pores (black). In (**B**), plates and cement can be differentiated—coccolithophore plate = pale grey; calcite cement = darker grey. Therefore, original porosity is greater than apparent in (**A**). Further, the pore-filling microquartz cement is shown (bright grain, bottom right (**B**)).
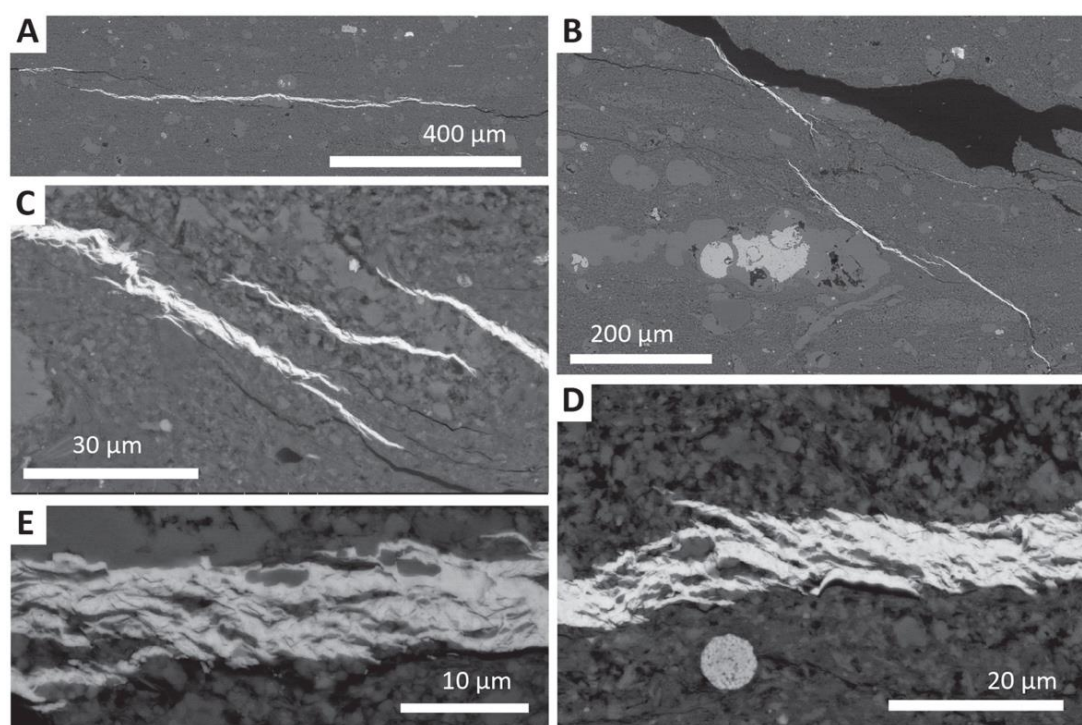
Figure 8. Examples of baryte-bearing anastomosing microfractures within the mudstone matrix. (**A**,**B**) Horizontal and inclined examples. (**C**) Example of three en echelon inclined microcracks. (**D**,**E**) Details of horizontal microcracks, with en echelon and anastomosing veinlets.

4. Discussion

Previous geochemical work [13] indicates that the La Cristalina mudstones were deposited in a high-productivity environment, with relative enrichment in Mo, V, U, and Zn, and high Zn/Al, Cu/Al, and Ni/Al ratios. High productivity is further supported by the abundance of foraminifera tests and the occurrence of faecal strings containing coccolithophore plates (Figures 1 and 7). The occurrence of calcite cements, as well as sulphide and sulphate species within the chambers of foraminifera, may have a number of important consequences that should be taken into consideration when considering environmental settings, and applying interpretations of bulk collected geochemical data.

4.1. Significance of Authigenic Mineral Formation

4.1.1. Calcite

The occurrence of large amounts of authigenic calcite within the chambers of foraminifera has the potential to greatly raise the total carbonate budget of such mudrock. Standard geochemical assay techniques, X-ray fluorescence (XRF) and X-ray diffraction (XRD) do not differentiate biological (primary) calcite from authigenic calcite. Therefore, without additional information, for example, from thin-section analysis (optical or SEM), the amount of primary biological calcite may well be overestimated. This is comparable to the situation of microquartz development within mudstones illustrated by Buckman et al. [13]. A typical area of La Cristalina shale (Figure 9A) has approximately 13% calcite, which comprises both biological calcite (foraminifera tests and coccolithophore plates) and later authigenic calcite cement. If a contribution to the carbonate budget from coccolithophore plates is excluded, then dependant on foraminifera morphology (Figure 9B,C), the difference in calcite percentage between uncemented and cemented foraminifera morphotypes could vary between 1/6th and 1/8th (Figure 9B–E), suggesting that original biocalcite levels could have been in the range of ~2%, considerably lower than the recorded value (13%). In this example, faecal pellets comprising disarticulated coccolithophore plates (Figure 7) also contribute to the overestimation of primary calcite

budget due to the occurrence of syntaxial calcite overgrowths (Figure 7B)—observed using the charge contrast imaging technique [14]. Overestimation of the primary biological calcite is of significance, as this will affect estimation of changes in rates of productivity, primary producer community, as well as how the mudrock is classified (i.e., calcareous, siliceous, terrigenous, etc.). For some materials, if the presence of authigenic cement is not recognised and taken into account, carbon and oxygen isotope analysis will be compromised, affecting, for example, estimates of seawater temperature [16,17]. In addition, the elemental composition of cements may differ radically from that of the primary biogenic calcite, depending on the timing of cement emplacement and fluid composition. For example, enrichment in Mn, Fe, Mg or Sr [14,18], which could impact the study and interpretation of shell chemistry (high-/low-Mg calcite, aragonite), while cements that are compositionally similar to shelly material may not be recognised (unless using CCI or CL), leading to the masking of taxonomic criteria such as the presence and character of pore structures.
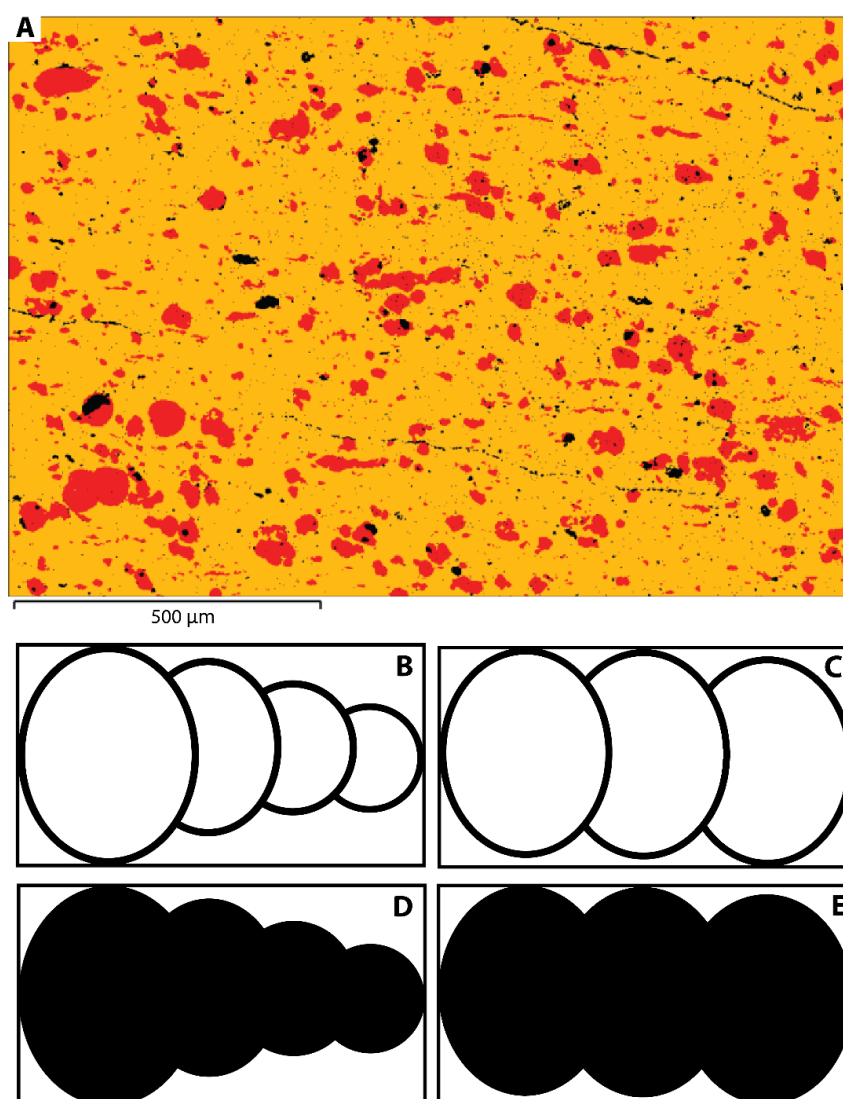
Figure 9. (**A**) Energy dispersive X-ray (EDX) phase image of a representative area of La Cristalina shale. Orange = shale matrix; red = calcite (foraminifera, coccolithophore plates within faecal pellets and calcite cement). (**B**,**C**) Schematic illustrations of simple uniserial foraminifera morphology (used to simplify analysis). Black = foraminifera test; approximately 11% in each case. (**D**,**E**) As in (**B**,**C**), with the addition of calcite cement fill. Black = test and calcite cement; approximately 68% and 82%. In all cases, percentage calcite calculated by simple image analysis binary thresholding.

4.1.2. Sphalerite

Zinc is a particularly important element used in geochemical interpretation of environmental change, with the Zn/Al ratio being used to assess relative enrichment or depletion in respect to average shale [19,20]. The Zn/Al ratio for the sample examined and associated analysed samples of 67.53 and 254.92 [13] is high, even in comparison to other related high-productivity shales such as those from the Zipa section in Colombia [13], which is in line with generally high Zn/Al ratios in Cretaceous shales and mudstones [20]. In the current case, given the co-occurrence of pyrite replacing opaline sponge spicules, which have previously been recorded as sources of Zn and Ba in areas of high productivity and upwelling [13,21], and the high degree of early microquartz cement [13], it is likely that both sphalerite and baryte were produced during the early stages of burial (eogenesis)—preserving the environmental signal of high-productivity upwelling waters—although it cannot be excluded that anomalously high Zn/Al values may be due to the concentration of sphalerite within foraminifera chambers. The preferential formation and the concentration of sphalerite within foraminifera tests may in part be due to the occurrence of organic matter, as zinc and organic carbon have previously been shown to be positively correlated [22], and Zn held within organometallic complexes can be released under reducing conditions and incorporated either in pyrite or form sphalerite [23]. It should also be noted that in Figure 3B, sphalerite seems to occur around pyrite framboids and was therefore precipitated later. This could be due to decreasing hydrogen sulphide concentrations in the ambient pore waters/within the foraminiferal chamber, since sphalerite has a tendency to form at such lower hydrogen sulphide levels [24]. The relative significance of such localised concentrations will depend on the extent to which the system is closed, the type and extent of available pathways for fluid/ion migration, and the scale/resolution that measurements are taken at.

4.1.3. Baryte

Barium can have a hydrothermal [25,26] as well as biogenic or detrital origin [21,27–30]. While the origin of biogenic-derived barium is still not fully resolved, recent research supports the idea of baryte precipitation in supersaturated microenvironments within organic particles sinking down through the water column [31], but it has also been associated with siliceous microorganisms in oxygenated waters of coastal upwelling areas [21]. A number of authors have positively correlated excess non-lithogenic (biogenic) barium with water depth with higher concentration at water depths greater than 1000 m [28,30]. Diagenetic dissolution of baryte is commonly observed in marine sediments where pore waters are depleted in sulphate, followed by reprecipitation of authigenic baryte when sulphate becomes available again [28]. In addition, during early diagenesis, dissolution of opaline biogenic quartz is known to result in the high concentration of barium in pore waters [29]. Given the association of pyrite replaced siliceous sponge spicules from the current sample (Figure 10), it is possible that baryte within foraminifera chambers has a biogenic origin, with baryte precipitated from Ba-enriched pore waters (during eogenesis), associated with a deep-water high-productivity environment of deposition. Nevertheless, a hydrothermal origin for such materials is equally possible. It is remarkable that high-resolution mapping of baryte occurrence (Figure 5) shows no preferential enrichments of baryte within the scanned samples, in stark contrast to pyrite and sphalerite, instead being pervasively developed throughout. This may indicate that supersaturated microenvironments leading to primary baryte formation might have occurred within foraminifera tests themselves, or such conditions developed following the burial of the tests into deeper sediments. Baryte formation in large fractures is easily observed [26], and therefore avoided, in geochemical surveys for environmental analysis, whereas the same could not be readily said for baryte within foraminifera chambers (which is also equally valid for sphalerite). At least some of the observed baryte may be late (remobilised) and associated with uplift and unloading (telogenesis), although given the occurrence of basin foreshortening (see below), it may have formed during burial (mesogenesis) associated with the formation of bedding parallel cracks. Therefore, it is feasible that baryte within foraminifera chambers, and microcracks, could have formed at any stage from eogenesis, through mesogenesis to late telogenesis, or indeed all three. Consequently,

the recording of these or other shales as strongly Ba enriched in such cases may not be representative of the shale as a whole and may be of uncertain affinity and of dubious specific environmental significance. In such cases, further detailed sedimentological observation paired with high-resolution geochemical analysis would be beneficial to elucidate the exact origins of the formation of baryte, and barium-rich fluids, in order to support any detailed geochemical/environmental interpretation.
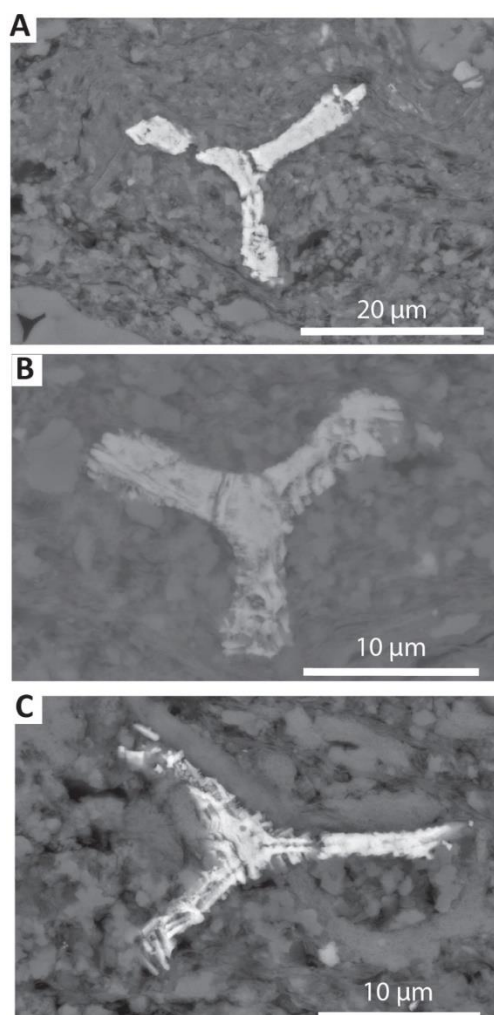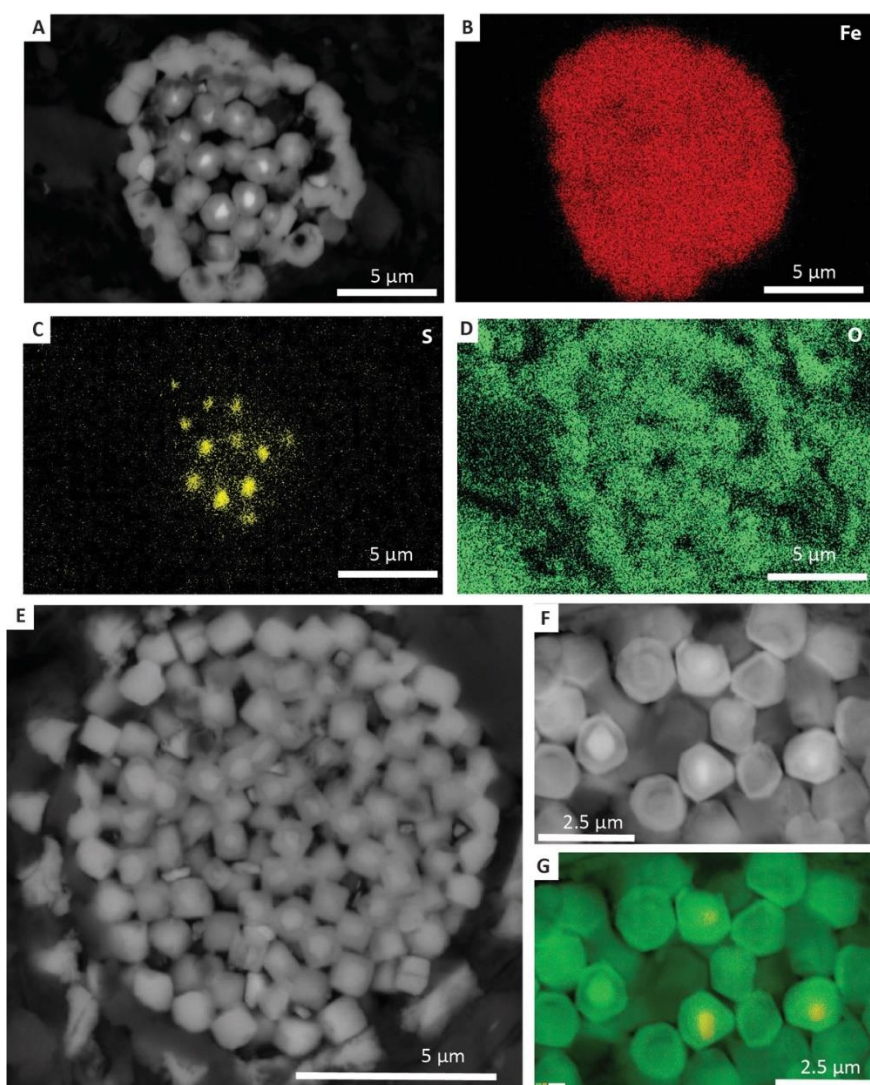

Figure 10. Backscattered electron (BSE) images, illustrating the typical form of siliceous sponge spicules replaced by pyrite. (**A–C**) showing slight variations in morphology and pyritization.

4.1.4. Pyrite/Fe Oxides

Timing of pyrite (FeS_2) framboid formation and, by inference, the later more massive surrounding forms is uncertain. It is possible that the framboids grew in association with organic material within the foraminifera chamber, possibly within the water column prior to burial, or soon after burial near to the seafloor sediment interface. Notably, FeS_2 is known to occur in two forms—pyrite (cubic) and marcasite (orthorhombic)—and euhedral crystals of marcasite are often found associated with framboids of pyrite, which they may surround [32]. Such changes in morphology are postulated as recording temporary changes in redox levels, specifically lower pH and more oxidising conditions [32]. Differentiation of pyrite and marcasite is difficult, and morphological comparison with previously recorded materials is not conclusive. Ideally, electron backscatter diffraction (EBSD) would resolve this question, but was not available for this study. The presence of marcasite is of particular interest, as this is at odds with the conditions required for the formation of pyrite, sphalerite and baryte. However, this may reflect changes in oxygenation in the water column or sea floor, fluctuating between reducing (anoxic/sulphidic) and

oxic conditions, followed by increased anoxia during burial. The occurrence of altered framboids and euhedral forms of FeS_2 to Fe oxides (Figure 11) represents subsequent oxidation, either during uplift and subsequent weathering, or possibly influenced by a change to more oxidising conditions during burial. The former seems more likely, given the assumed reduced permeability likely after compaction and the early stages of diagenesis, and given that the iron oxides form in a halo around the main area of pyrite distribution (cf [33]; Figures 5 and 11). The iron sulphide/oxide species noted within the foraminifera and mudstone matrix therefore record a range of geochemical changes throughout different periods of the mudstones depositional to burial and subsequent uplift/weathering history.


Figure 11. Examples of oxidised pyrite framboids. (**A**) Backscattered electron (BSE) image of badly altered pyrite framboid. Bright points are unaltered pyrite framboid microcrystal cores; darker grey areas are depleted in sulphur and oxidised. (**B–D**) Energy dispersive X-ray (EDX) maps of the area in (**A**), for Fe, S and O, respectively. (**E**) A better-preserved pyrite framboid, but still heavily altered as in (**A**). (**F,G**) Detailed BSE and EDX map of an altered pyrite framboid (similar to (**E**)). In (**F**), variations in grey scale reflect different degrees of loss of S and oxidation (see Mahoney et al. [33]). Note that (**G**) is a composite map for O and S. Oxidised areas appear green and more pristine pyrite "cores" are yellow.

4.1.5. Foraminifera Chamber vs. Shale Matrix Diagenesis

Interestingly, the authigenic processes that occur within the foraminifera are different in character to those within the mudstone matrix. Authigenic processes within the mudstone matrix, while

including the formation of pyrite framboids, do not include the formation of marcasite, sphalerite or baryte, but instead are dominated by the formation of microquartz [13], which occurs to a much lesser extent within foraminifera. This suggests that the geochemical microenvironments between mudstone matrix "micro" porosity and foraminifera chamber "macro" porosity, and potentially the mechanisms for fluid migration, are significantly different at the small sediment layer scale to promote the observed variance in mineral species. In the case of pyrite and sphalerite, this may be mitigated by the presence of reactive organic matter. This work agrees with that of Camp [10], who indicated that foraminifera chambers, within the contemporaneous Eagle Ford Formation of Texas, can act as crucibles for the study of diagenetic products (e.g., pyrite, quartz, calcite and kaolinite) resulting from thermo-chemical reactions during burial, and that diagenesis can be different between foraminifera chambers and normal pore spaces. Therefore, detailed analysis of the type and timing of such diagenetic products (within foraminifera chambers—Figure 12) and comparison to cements within other mudstone matrix porosities should be formative in determining details of changes in fluid movement, dissolution and mineral diagenesis brought about during burial (mesogenesis) and subsequent uplift (telogenesis). The understanding and differentiation of the authigenic processes within shale matrix compared to that of unusual microcrucibles, such as within foraminifera, should be taken into consideration, especially where geochemical data is extracted to interpret a range of environmental factors, including productivity, water depth and anoxia amongst others.
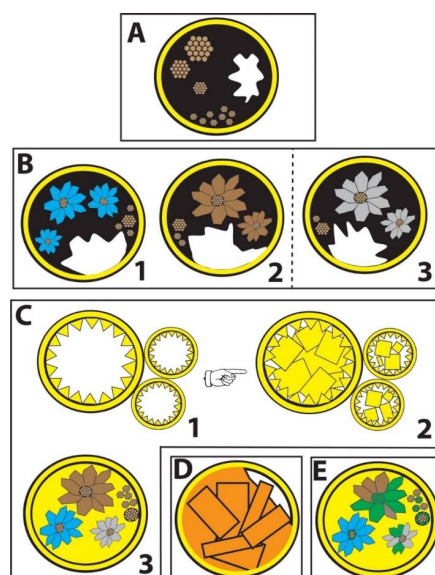
Figure 12. Schematic cartoon of diagenetic sequence observed within foraminifera tests within the studied material. (**A**) Initial formation of pyrite framboids, probably in association with organic matter (black), either in water column, or during early burial. Anoxic or dysaerobic conditions. (**B**) Formation of euhedral species surrounding some of the pyrite framboid cores: 1—sphalerite (reducing environment); 2—pyrite (reducing environment); 3—"marcasite" (temporary change to more acidic and oxidising conditions). Zn for sphalerite, derived from dissolution of siliceous (opaline) microorganisms (sponge spicules) within mudstone matrix—spicules pyritised. (**C**) Formation of calcite cements, with two major phases. 1—Fine internal; 2—later coarser sparry cement, infilling chambers (and reducing porosity); 3—resulting in sulphide phases embedded within calcite. (**D**) Formation of later-stage pervasive baryte in foraminifera tests and horizontal microcracks, in association with basin foreshortening, sequence thickening and major thrusting. Barium possibly sourced from dissolution of opaline sponge spicules, and later remobilised, or associated with the migration of hydrothermal fluids during thrusting. (**E**) Uplift and weathering, resulting in partial and variable degree of oxidation of FeS_2, both framboids and equant crystals. Note crystal shapes illustrated are not morphologically accurate, but rather indicative of phase distribution. Brown = pyrite; blue = sphalerite; green = oxidised FeS_2 (pyrite or marcasite); grey = marcasite; orange = baryte; yellow = calcite; solid black = organics.

4.2. Significance of Test Damage

The missing lateral margins of the foraminifera test can be hypothesised to have a number of origins: (i) predatory damage; (ii) natural marginal collapse, brought about during burial; (iii) shell damage caused during transportation; or (iv) localised dissolution.

4.2.1. Predation

Active predation of foraminifera could conceivably cause damage to the test. However, given the small size of the foraminifera affected, and the localisation of damage to the margins of the test, it is hard to envisage either the instigator or the purpose of such specific damage. In addition, unless damage is caused all around the periphery of the test, an additional mechanism is required to explain the alignment of tests, so that the damage is commonly observed in the plane of the thin section.

4.2.2. Shell (Test) Collapse

Where foraminifera, or other structures, are variable in architecture, some parts may be structurally more robust than others; with spherical structures possessing higher load-bearing capacity than more tapered slender structures. However, in this case, the foraminifera appear robust enough to withstand burial loading (vertical compaction), and in many cases, are further supported by internal strengthening through the precipitation of authigenic minerals such as calcite, pyrite, sphalerite and baryte. In addition, there is no evidence to suggest that the lateral peripheries were architecturally different to the rest of the foraminiferal test, and therefore less robust.

4.2.3. Transportation Damage

If it is hypothesised that tests were deposited from an ocean current, it may be possible to explain the damage as due to transportation. Similar stringers of foraminifera, and faecal material containing disarticulated coccolith plates (Figures 1 and 7) can appear similar to bioclastic material transported and deposited by bottom currents [5], but lack characteristic erosive basal surfaces. Additionally, if damage was in this case explained by entrainment and transportation in bottom currents flowing along the sea floor, then evidence of abrasion might reasonably be expected throughout the tests periphery, which is not generally the case.

4.2.4. Localised Dissolution

The samples examined were deposited within a deep-water basin that currently sits within an active thrust belt zone, at the margin of the Eastern Cordillera, and is marked by crustal thickening and structural foreshortening [34–36], and in particular, the site is located between two thrust faults (Figure 2). Given this, the lateral damage potentially can be explained as the product of localised dissolution brought about by lateral compression (foreshortening). This is indicated by the association of early microquartz with the damaged areas (Figures 4 and 6), with the microquartz (and silt sized detrital particles) being pushed into calcite cement and shell during the dissolution process.

4.2.5. Overview of Test Damage

None of the above hypotheses unequivocally explain the damage patterns observed. However, localised dissolution due to basin foreshortening appears to be the most likely explanation. Lithologically, mudstones such as the Eagle Ford Formation come from similar deep-water settings with high numbers of foraminifera and faecal lenses. However, there appears to be no mention of test damage within the literature, and none have been personally observed by the authors from representative examined materials. This is perhaps surprising, as the Eagle Ford has also undergone basin compression during the Larimide Orogeny [37].

5. Conclusions

Foraminifera host a range of authigenic minerals (calcite, pyrite, sphalerite and baryte) which hold clues to the composition and timing on the migration of fluids through mudrocks. The example illustrated in this study demonstrates the potentially complex geochemical and authigenic history of a foraminiferal-rich mudstone, during deposition, burial, and uplift, that can be hidden away within such foraminifera (Figure 12), and may radically differ from that observed within shale matrix materials. This is in agreement with previous studies [10]. It also illustrates how apparently simple forms of foraminifera test damage can be interpreted in a range of ways, from ecological, environmental, taphonomic scenarios, to evidence of structural foreshortening. Although much can often be gleaned from the examination of such materials, it is not always an easy task to separate out the exact meaning and timing of all events that have taken place. Knowledge of such hidden pockets of information may provide additional details on burial and diagenesis, while ignorance may impact on whole rock-derived geochemical analysis of environmental change indices, particularly in respect to both Ba and Zn. Further work on materials within the Eastern Cordillera, and other environmental-time equivalents (e.g., Eagle Ford Formation), and mudstones in general, may prove informative, with the potential to obtain big things out of small.

Author Contributions: Conceptualisation, J.B.; methodology, J.B. and C.M. (Carol Mahoney); formal analysis, J.B.; investigation, J.B.; resources, J.B.; writing—original draft preparation, J.B.; writing—review and editing, J.B., T.W. and C.M. (Christian März); supervision, J.B., T.W., and C.M. (Christian März). All authors have read and agreed to the published version of the manuscript.

References

1. Kaminski, M.A.; Schroder, C.J. Environmental analysis of deep-sea agglutinated foraminifera: Can we distinguish tranquil from disturbed environments? In Proceedings of the Gulf Coast Section SEPM Foundation Proceedings of the 8th Annual Research Conference, Houston, TX, USA, 3–6 December 1987; pp. 90–93.

2. Kaminski, M.A.; Boersma, A.; Tyszka, J.; Holbourn, A.E.L. Response of deep-water agglutinated foraminifera to dysoxic conditions in the California Borderlands basins. In *Proceedings of the Fourth International Workshop on Agglutinated Foraminifera, Kraków, Poland, 12–19 September 1993*; Kaminski, M.A., Geroch, S., Gasinski, M.A., Eds.; Grzybowski Foundation: Krakow, Poland, 1995; pp. 131–140.

3. Kucera, M. Planktonic Foraminifera as Tracers of Past Oceanic Environments. In *Developments in Marine Geology*; Elsevier: Amsterdam, The Netherlands, 2007; pp. 213–262. ISSN 1572-5480.

4. Schieber, J. Discovery of agglutinated benthic foraminifera in Devonian black shales and their relevance for the redox state of ancient seas. *Paleogeogr. Paleoclimatol. Paleoecol.* **2009**, *271*, 292–300. [CrossRef]

5. Schieber, J.; Southard, J.B.; Schimmelmann, A. Lenticular shale fabrics resulting from intermittent erosion of water-rich muds—Interpreting the rock record in the light of recent flume experiments. *J. Sed. Res.* **2010**, *80*, 119–128. [CrossRef]

6. Schieber, J. Styles of agglutination in benthic foraminifera from modern Santa Barbara Basin sediments and the implications of finding fossil analogs in Devonian and Mississippian black shales. In *Anoxia: Evidence of Eukaryote Survival and Paleontological Strategies*; Altenbach, A.V., Bernard, J.M., Seckbach, J., Eds.; Springer Science: Berlin/Heidelberg, Germany, 2011; pp. 573–590.

7. Flores, J.A.; Johnson, J.E.; Mejía-Molina, A.E.; Álvarez, M.C.; Sierro, F.J.; Singh, S.D.; Mahanti, S.; Giosan, L. Sedimentation rates from calcareous nannofossil and planktonic foraminifera biostratigraphy in the Andaman Sea, northern Bay of Bengal, and eastern Arabian Sea. *Mar. Pet. Geol.* **2014**, *58*, 425–437. [CrossRef]

8.　Stefanoudis, P.V.; Schiebel, R.; Mallet, R.; Durden, J.M.; Bett, J.B.; Gooday, A.J. Agglutination of benthic foraminifera in relation to mesoscale bathymetric features in the abyssal NE Atlantic (Porcupine Abyssal Plain). *Marine Micropaleontol.* **2015**, *123*, 15–28. [CrossRef]

9.　Doering, K.; Erdem, Z.; Ehlert, C.; Fleury, S.; Frank, M.; Schneider, R. Changes in diatom productivity and upwelling intensity off Peru since the Last Glacial Maximum: Response to basin-scale atmospheric and oceanic forcing. *Paleoceanography* **2016**. [CrossRef]

10.　Camp, W. Diagenesis of organic-rich shale: Views from foraminifera *Penetralia*, Eagle Ford Formation, Maverick Basin, Texas. In Proceedings of the AAPG Rocky Mountain Section Meeting, Denver, CO, USA, 20–22 July 2014.

11.　Ramiro-Ramirez, S. Petrographic and Petrophysical Characterization of the Eagle Ford Shale in La Salle and Gonzales Counties, Texas. Master's Thesis, Colorado School of Mines, Golden, CO, USA, 2016.

12.　McAllister, R.T. Diagenetic Modifications of the Eagle Ford Formation: Implications on Chemical and Physical Properties. Ph.D. Thesis, University of Manchester, Manchester, UK, 2017.

13.　Buckman, J.; Mahoney, C.; März, C.; Wagner, T.; Blanco, V. Identifying biogenic silica: Mudrock micro-fabric explained through charge contrast imaging. *Am. Miner.* **2017**, *102*, 833–844. [CrossRef]

14.　Buckman, J.O.; Corbett, P.W.M.; Mitchell, L. Charge contrast imaging (CCI): Revealing enhanced diagenetic features of a coquina limestone. *J. Sed. Res.* **2016**, *86*, 734–748. [CrossRef]

15.　Giuliani, G.; Groat, L.A.; Marshall, D.; Fallick, A.E.; Branquet, Y. Emerald deposits: A review and enhanced classification. *Minerals* **2019**, *9*, 105. [CrossRef]

16.　Branson, O.; Read, E.; Redfern, S.A.T.; Rau, C.; Elderfield, H. Revisiting diagenesis on the Ontong Java Plateau: Evidence for authigenic crust precipitation in *Globorotalia tumida*. *Paleoceanography* **2015**. [CrossRef]

17.　Davis, C.V.; Fehrenbacher, J.S.; Hill, T.M.; Russell, A.D.; Spero, H.J. Relationships between temperature, pH, and crusting on Mg/Ca ratios in laboratory-grown Neogloboquadrina foraminifera. *Paleoceanography* **2017**. [CrossRef]

18.　Boggs, S., Jr.; Krinsley, D. *Applications of Cathodoluminescence Imaging to the Study of Sedimentary Rocks*; Cambridge University Press: Cambridge, UK, 2006; 165p.

19.　Wedepohl, K.H. Environmetal influences on the chemical composition of shales and clays. *Phys. Chem. Earth* **1971**, *8*, 305–333. [CrossRef]

20.　Brumsack, H.J. The trace metal content of recent organic carbon-rich sediments: Implications for Cretaceous black shale formation. *Palaeogeogr. Palaeoclimatol. Palaecol.* **2006**, *232*, 344–361. [CrossRef]

21.　Jewell, P.W.; Stallard, R.F. Geochemistry and Paleoceanographic Setting of Central Nevada Bedded Barites. *J. Geol.* **1991**, *99*, 151–170. [CrossRef]

22.　Desborough, G.A.; Hatch, J.R.; Leventhal, J.S. Geochemical and mineralogical comparison of the Upper Pennsylvanian Stark Shale Member of the Dennis Limestone, East-Central Kansas, with the Middle Pennsylvannian Mecca Quarry Shale Member of the Carbondale Formation in Illinois and of the Linton Formation in Indiana. *US Geol. Surv. Circ.* **1989**, *1058*, 12–30.

23.　Tribovillard, N.; Algeo, T.J.; Lyons, T.; Riboulleau, A. Trace metals as paleoredox and paleoproductivity proxies: An update. *Chem. Geol.* **2006**, *232*, 12–32. [CrossRef]

24.　Morse, J.W.; Luther, G.W., III. Chemical influences on trace metal-sulfide interactions in anoxic sediments. *Geochim. Cosmochim. Acta* **1999**, *63*, 3373–3378. [CrossRef]

25.　Bloomstein, E.I.; Clark, J.B. Geochemistry of the Ordovician high-calcium black shales hosting major gold deposits of the Getchell Trend in Nevada. *US Geol. Surv. Circ.* **1989**, *1058*, 1–5.

26.　Elmore, R.D.; Dulin, S.A.; Manning, E.B.; Steullet, A.K.; Benton, A.; Dennie, D.; Roberts, J.; Heij, G.; Deng, J. Paragenesis of Mineralized Fractures in Organic Rich Shales. In Proceedings of the AAPG Annual Convention and Exhibition, Denver, CO, USA, 31 May–3 June 2015.

27.　Bishop, J.K.B. The barite-opal-organic carbon association in oceanic particulate matter. *Nature* **1988**, *332*, 341–343. [CrossRef]

28.　Von Breymann, M.T.; Emeis, K.C.; Suess, E. Water depth and diagenetic constraints on the use of barium as a paleoproductivity indicator. In *Upwelling Systems: Evolution since the Early Miocene*; Summerhayes, C.P., Prell, W.L., Emeis, K.C., Eds.; The Geological Society: London, UK, 1992; pp. 273–284.

29.　Torres, M.E.; Brumsack, H.J.; Bohrman, G.; Emeis, K.C. Barite front in continental margin sediments: A new look at barium remobilization in the zone of sulfate reduction and formation of heavy barites in diagenetic fronts. *Chem. Geol.* **1996**, *127*, 125–139. [CrossRef]

30. Hetzel, A.; März, C.; Vogt, C.; Brumsack, H.-J. Geochemical environment of Cenomanian-Turonian black shale deposition at Wunstorf (northern Germany). *Cret. Res.* **2011**, *32*, 480–494. [CrossRef]

31. Martinez-Ruiz, F.; Paytan, A.; Gonzalez-Muñoz, M.T.; Jroundi, F.; Abad, M.M.; Lam, P.J.; Bishop, J.K.B.; Horner, T.J.; Morton, P.L.; Kastner, M. Barite formation in the ocean: Origin of amorphous and crystalline precipitates. *Chem. Geol.* **2019**, *511*, 441–451. [CrossRef]

32. Schieber, J. Marcasite in Black Shales—A Mineral Proxy for Oxygenated Bottom Waters and Intermittent Oxidation of Carbonaceous Muds. *J. Sed. Res.* **2011**, *81*, 447–458. [CrossRef]

33. Mahoney, C.; März, C.; Buckman, J.; Wagner, T.; Blanco-Velandia, V.-O. Pyrite oxidation in shales: Implications for palaeo-redox proxies based on geochemical and SEM-EDX evidence. *Sed. Geol.* **2019**, *89*, 186–199. [CrossRef]

34. Mora, A.; Horton, B.K.; Mesa, A.; Rubiano, J.; Ketcham, R.A.; Parra, M.; Blanco, V.; Garcia, D.; Stockli, D.F. Migration of Cenozoic deformation in the Eastern Cordillera of Colombia interpreted from fission track results and structural relationships: Implications for petroleum systems. *AAPG Bull.* **2010**, *94*, 1543–1580. [CrossRef]

35. Parra, M.; Mora, A.; Jaramillo, C.; Torres, V.; Zeilinger, G.; Strecker, M.R. Tectonic controls on Cenozoic foreland basin development in the north-eastern Andes, Colombia. *Basin Res.* **2010**, *22*, 874–903. [CrossRef]

36. Bande, A.; Horton, B.K.; Ramírez, J.C.; Mora, A.; Parra, M.; Stockli, D.F. Clastic deposition, provenance, and sequence of Andean thrusting in the frontal Eastern Cordillera and Llanos foreland basin of Colombia. *Geol. Soc. Am. Bull.* **2012**, *124*, 59–76. [CrossRef]

37. Gottardi, R.; Mason, S.L. Characterization of the natural fracture system of the Eagle Ford Formation (Val Verde County, Texas). *AAPG Bull.* **2018**, *102*, 1963–1984. [CrossRef]